

## Tuning the dielectric and structural properties of erbium substitution on cobalt ferrites

H. M. N. H. K. Asghar<sup>a</sup>, M. Hussain<sup>a</sup>, S. Aslam<sup>a</sup>, Z. A. Gilani<sup>a,\*</sup>, M. S. Ahmed<sup>b</sup>, M. Khalid<sup>d</sup>, M. S. Shifa<sup>c</sup>, M. Afzal<sup>c</sup>

<sup>a</sup>*Department of Physics, Balochistan University of Information Technology, Engineering & Management Sciences, Quetta 87300, Pakistan.*

<sup>b</sup>*Department of Computer Science and Information Technology, Govt. Sadiq College Women University, Bahawalpur, Pakistan*

<sup>c</sup>*Institute of Physics, The Islamia University of Bahawalpur, Pakistan.*

<sup>d</sup>*Department of Physics, University of Karachi, Pakistan*

Spinel ferrites having the composition  $\text{CoEr}_x\text{Fe}_{2-x}\text{O}_4$  ( $x = 0.0, 0.01, 0.02, 0.03, 0.04, 0.05$ ) was synthesized through micro emulsion method. To study the structural, IR spectra, morphology and composition and electrical properties of these spinel ferrites, the characterization of samples was done by XRD, FTIR, SEM and Dielectric properties respectively. Spinel ferrites XRD patterns revealed that the structure was crystallite and single phase. By doping the rare earth metal Erbium, it was shown that there were variations in lattice parameters. The range of Crystallite size was in 19- 25nm which was calculated by Scherer formula. FTIR recorded the IR spectra, the absorption bands of IR spectra revealed that all samples were spinel ferrites. SEM also confirmed the shape of the particle and grain size that is found to be in agreement with the XRD data, it also showed monotony in the morphology. Real and imaginary parts of impedance  $Z'$  and  $Z''$  in the frequency range of 1MHz to 3 GHz was plotted. The results show that the impedance decreases with increasing frequency. In order to determine the grain effect, the real and imaginary parts electrical modulus was plotted with increasing Erbium substitution. The effect of frequency in high frequency region gives the variation in electrical modulus. Furthermore, real and imaginary parts of dielectric constant were plotted as a function of frequency. The results show the significant effect in the high frequency region. Also the same behavior was observed in case of tangent loss. Ac conductivity was determined showing the increasing trend with increasing frequency. Excellent dielectric properties suggest that  $\text{Er}^{3+}$  has significant effects for the application of high frequency devices.

(Received April 22, 2021; Accepted August 10, 2021)

**Keywords:** Co-ferrite, Erbium, Nanocrystallite ferrites, XRD, Microemulsion, Dielectric properties

### 1. Introduction

In the modern world magnetic materials are the key factors in technology. The importance of ferrites has been realized for many centuries by human by studying their different properties [1]. Development of ferrites depends mainly on the advancement and the development of the techniques. Chemical composition, annealing and the doped metal ions can control different properties of ferrites such as magnetization, electrical conductivity and permittivity, and dielectric losses [2, 3]. The spinel ferrites have the most popular magnetic and electrical properties [4]. Due to its high electrical resistance capability such types of material are well suited for They are used in microwave device application[5] and are highly expected candidate for a magneto-optical recording medium because of their distinctive magnetic properties[6, 7]. For magnetic recording media application, writing and overwriting of data are defined by the two important parameters as low hysteresis loss and thermal stability of the magnetic data bit. These both parameters are determined by lower blocking temperature[8], [9].

---

\* Corresponding author: zagilani2002@yahoo.com

Synthesis of some composites of multi-ferric materials was done by multiple means which are;  $\text{CoFe}_{2-x}\text{Gd}_x\text{O}_4$  synthesized by solid state reaction technique [10],  $\text{CoFe}_{2-x}\text{Hf}_x\text{O}_4$  synthesized by varying the amount of hafnium  $x = 0.0-0.2$  [11],  $\text{CoRE}_x\text{Fe}_{2-x}\text{O}_4$  doped by the chemical co-precipitation method [12],  $\text{CoY}_x\text{Fe}_{1.98-x}\text{O}_4$  developed using sol-gel combustion method [13],  $\text{CoHo}_x\text{Fe}_{2-x}\text{O}_4$  synthesized by co-precipitation method [14],  $\text{Na}_2\text{B}_4\text{O}_7 \cdot 10\text{H}_2\text{O}$  (Borax) as a solvent(flux)grown by the flux method [8].  $\text{CoFe}_{2-x}\text{Pr}_x\text{O}_4$  ranging from 0.025 to 0.10 were successfully prepared by the easy and free surface-assisted hydrothermal method [15],  $\text{CoMn}_x\text{Fe}_{2-x}\text{O}_4$  spinel ferrites nanoparticles were synthesized with the help of sol-gel technology [16].

In above all mentioned materials, the magnetic properties and magneto-elastic properties of Co ferrites were observed and investigated. Anisotropy coefficient, coercivity, magnetic properties and high strain sensitivity were found to be decreased by increasing the heat temperature, but the temperature is very effective parameter on magnetization as the magnetization decreases with increasing temperature. This change does not affect the crystal structure and composition. The cations distribution on the both lattice sites of A and B can change the magnetic and magneto-elastic properties of material [17].

In the present study, we have developed a  $\text{CoFe}_2\text{O}_4$  series by substitution of Er using the micro-emulsion method. We examined the different structural and electrical properties by changing the concentration.

## 2. Experimental Procedure

Microemulsion technique was used to synthesize  $\text{CoEr}_x\text{Fe}_{2-x}\text{O}_4$  ( $x = 0.0, 0.01, 0.02, 0.03, 0.04, 0.05$ ). This method is beneficial because it limits the nucleation of cations than other different methods like sol-gel and solid state method, Following chemicals were required for solution preparation Erbium oxide, Cobalt acetate tetra-hydrate( $(\text{CH}_3\text{COO})_2\text{Co} \cdot 4\text{H}_2\text{O}$ ), Iron nitrate nano-hydrate [ $(\text{Fe}(\text{NO}_3)_3 \cdot 9\text{H}_2\text{O})$ ], Cetyltrimethylammonium bromide (CTAB). The sample solutions of cobalt, erbium and iron were prepared in distilled water. The solution was putted on the hot plate and continuously stirred at temperature  $55^\circ\text{C}$ . CTAB solution was mixed in this solution. The PH was maintained till 10 by adding ammonia in the solution and then stirred till 5h. In order to remove the impurities and ammonia, the precipitate were wash by distill water to settle down  $\text{Fe}_2\text{O}_3$ . The solutions get neutralized after several times of washing. Removal of water was done in an oven at about  $100^\circ\text{C}$ . Annealing was done of each sample at  $950^\circ\text{C}$  in a muffle Vulcan A-550 furnace. The annealed material was then ready for characterization to study their properties.

Philips X'Pert PRO 3040/60 diffractometer and Nexus 470 spectrometer were used to investigate the XRD and FTIR patterns of all samples of  $\text{CoEr}_x\text{Fe}_{2-x}\text{O}_4$  ( $x = 0.0, 0.01, 0.02, 0.03, 0.04, 0.05$ ) respectively. The range of FTIR spectra was  $400-700\text{cm}^{-1}$ .

## 3. Results and Discussion

### 3.1. XRD analysis

Figure 1 shows magnified XRD patterns for cobalt ferrites with Er-doped. Diffraction peaks at (220), (311), (400), (420), (422), and (511) confirmed the desired spinel ferrites nanoparticles [JCPDS card # 22-1086][18]. It is clearly shown in Figure 1 that peak (311) shifted towards higher  $2\theta$ , which is due to the replacement of rare earth cation with Fe[19]. Er cations have larger radii and heavy mass as compare with Fe cations. With the increase of Er ion substitution, it is clearly shown in figure that secondary phases are investigated as with amount of ortho ( $\text{ErFeO}_3$ ) and hematite ( $\text{Fe}_2\text{O}_3$ ). In addition, the reason of the formation of these secondary may be due to the electronic configuration of  $\text{Er}^{3+}$  and also due to large ionic radii. Because of its larger ionic radii ( $1.03\text{\AA}$ ), Er prefers octahedral (12k, 4f2, 2a) sites of  $\text{Fe}^{3+}$  having ionic radii of  $0.67\text{\AA}$ . As a result there is development of other secondary phases appears due to inhomogeneity of  $\text{Er}^{3+}$  ions. Similar behavior have been investigated the development of secondary phases in the cubic spinel ferrites[20, 21].

The Er ions change the Fe<sup>3+</sup> ions in the A site consecutively, which as a result also increased the lattice parameter with the Er content[3]. With the increase of concentration from 0.00 to 0.05, it was found that crystalline structure of Er was weakening.

To determine the Lattice parameter “a”, below equation was used

$$a = d (h^2 + k^2 + l^2)^{1/2} \quad (1)$$

where the symbol ‘d’ represents the inter-planer spacing and index of XRD reflection peak is *hkl*

With increasing the concentration of Er, there is a lattice constant decrease then it varied as increasing and decreasing with the variation of concentration as shown in Figure 2. The variation in lattice parameter has been observed with respect to the substitution of Er<sup>3+</sup> because of its greater ionic radii as to ionic radii of Fe<sup>3+</sup>[22].

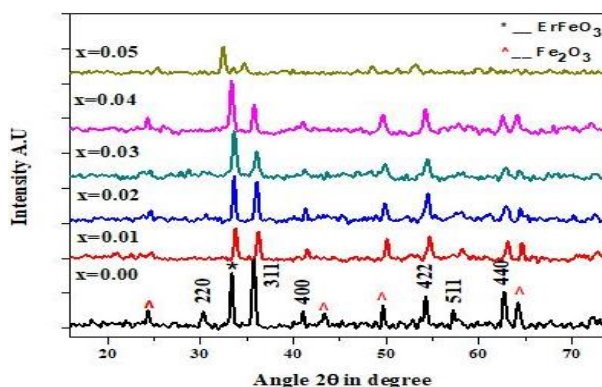


Fig. 1. XRD spectra of Erbium substituted cobalt ferrites nanoparticles

The formula used to find out the crystallite size is mentioned below

$$D = \frac{k\lambda}{\beta \cos\theta} \quad (2)$$

Where “k” has the constant value of 0.9,  $\lambda$  is the wave-length of X-ray beam. “ $\beta$ ” represents the Full Width Half Maxima (FWHM) and “ $\theta$ ” represents the diffraction angle of most intense peak.

Table 1. Different structural and physical parameters of  $\text{CoEr}_x\text{Fe}_{2-x}\text{O}_4$  ( $x = 0.0, 0.01, 0.02, 0.03, 0.04, 0.05$ ) spinel ferrites.

Parameter	X=0	X=0.01	X=0.02	X=0.03	X=0.04	X=0.05
Lattice constant(Å)	8.293	8.174	8.296	8.266	8.261	8.330
Cell volume(Å <sup>3</sup> )	570.465	546.200	571.043	564.924	563.787	578.201
Bulk density (gcm <sup>-3</sup> )	3.324	3.491	3.629	3.721	3.823	4.076
X-ray density(gcm <sup>-3</sup> )	5.051	5.303	5.096	5.180	5.216	5.112
Crystallite size (nm)	21.673	23.513	24.825	16.850	19.178	19.814

Crystallite size also showed variation when Er concentration was increased, which was in the range of 19nm to 25nm as show in Figure 3. This showed that Er is quite helpful in controlling the crystallite size. Figure 4 plotted between Er concentration and molecular weight shows that when Er concentration is increased, the molecular weight of samples also increased respectively. Bulk density with different concentration of Erbium was calculated by the following formula

$$D_x = 8M / Na^3 \quad (3)$$

Where  $M$  represents the *sample's molecular weight*  $N$  represents Avogadro's number which has value of  $6.0223 \times 10^{23}$  atoms/mole and " $a$ " is the lattice constant.

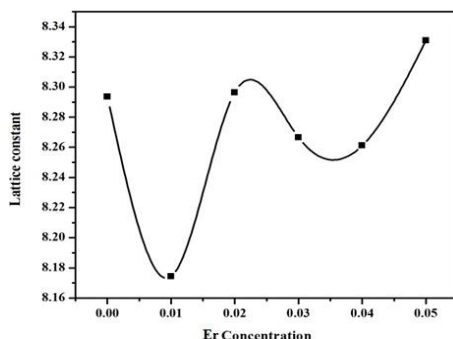


Fig. 2. Curve between lattice constant Vs Er concentration of  $\text{CoEr}_x\text{Fe}_{2-x}\text{O}_4$  ( $x = 0.0, 0.01, 0.02, 0.03, 0.04, 0.05$ ) spinel ferrites.

Bulk density was determined by formula is given as

$$p = m / V^3 \quad (4)$$

The trend in Figure 5 showed that the density (X-ray and Bulk) increased by increasing Erbium concentration. Table 1 exhibits the different structural parameters of  $\text{CoEr}_x\text{Fe}_{2-x}\text{O}_4$  ( $x = 0.0, 0.01, 0.02, 0.03, 0.04, 0.05$ ) spinel ferrites.

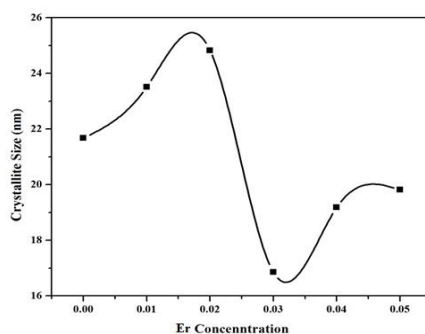


Fig. 3. curve between crystallite size VS Er concentration of  $\text{CoEr}_x\text{Fe}_{2-x}\text{O}_4$  ( $x = 0.0, 0.01, 0.02, 0.03, 0.04, 0.05$ ) spinel ferrites.

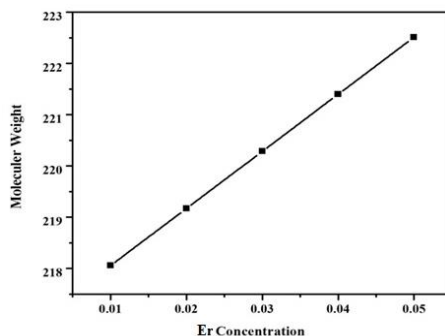


Fig. 4. Molecular weight and concentration of  $\text{CoEr}_x\text{Fe}_{2-x}\text{O}_4$  ( $x = 0.0, 0.01, 0.02, 0.03, 0.04, 0.05$ ) spinel ferrites.

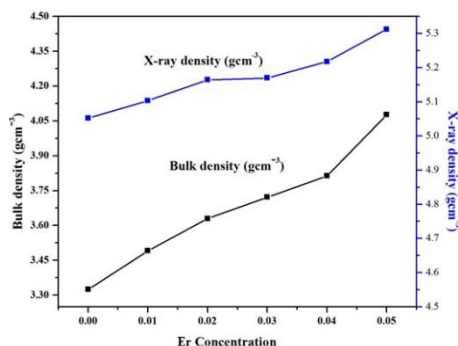


Fig. 5. X-ray and bulk density Vs Er concentration of  $\text{CoEr}_x\text{Fe}_{2-x}\text{O}_4$  ( $x = 0.0, 0.01, 0.02, 0.03, 0.04, 0.05$ ) spinel ferrites.

### 3.2. FTIR spectroscopy

FTIR spectra of  $\text{CoEr}_x\text{Fe}_{2-x}\text{O}_4$  ( $x = 0.0, 0.01, 0.02, 0.03, 0.04, 0.05$ ) is shown in Figure 6. Two main frequency bands were found in IR spectra of all spinel. The high frequency band  $\nu_1$  was around  $800\text{cm}^{-1}$  represent the intrinsic stretching of vibrations at the tetrahedral site, however low frequency band  $\nu_2$  was around  $500\text{cm}^{-1}$  which relates stretching at the octahedral sites. The bond stretching at the tetrahedral vibrations and bond bending type at the octahedral vibrations are determined by absorption frequency. The change in band position as a function of Erbium concentration is summarized in Table 2.  $\nu_1$  varied from  $558.42\text{cm}^{-1}$  to  $609.39\text{cm}^{-1}$  and  $\nu_2$  varied from  $524.49\text{cm}^{-1}$  to  $545.81\text{cm}^{-1}$ . The shift of  $\nu_1$  and  $\nu_2$  to this higher frequency band as the Er content increased was endorsed to the lattice constant variation. The variation in the lattice parameter had an effect on  $\text{Fe}^{+3}$ ,  $\text{O}^{2-}$  stretching vibrations by making a change in the band position [23].

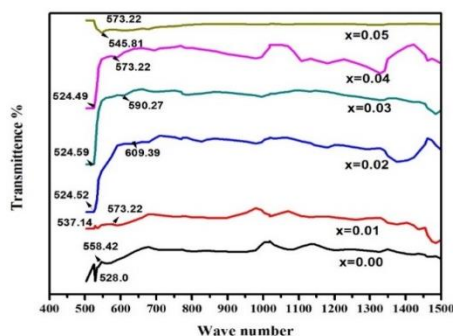


Fig. 6. FTIR spectra of  $\text{CoEr}_x\text{Fe}_{2-x}\text{O}_4$  ( $x = 0.0, 0.01, 0.02, 0.03, 0.04, 0.05$ ) spinel ferrites.

The force constant is very important parameters to study the variation in the octa and tetrahedral sites. These force constant for both sites can be calculated by the following formulas.

$$K_o = 0.94213 (v_2)^2 M / (M + 32) \quad (5)$$

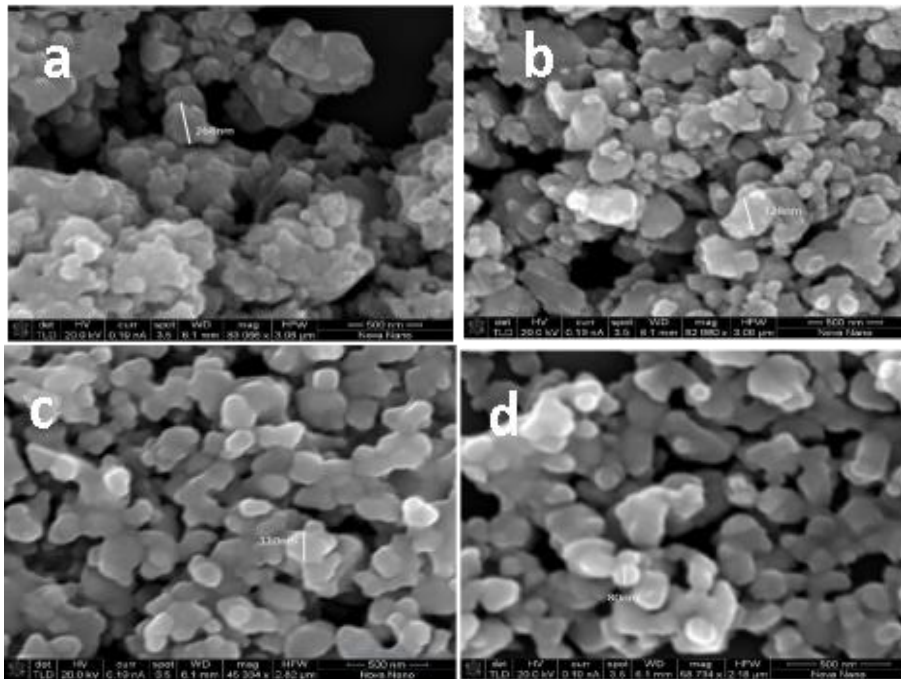
$$K_t = 2^{(1/2)} (v_1 / v_2) K_o \quad (6)$$

Table 2. Frequency bands of  $\text{CoEr}_x\text{Fe}_{2-x}\text{O}_4$  ( $x = 0.0, 0.01, 0.02, 0.03, 0.04, 0.05$ ) spinel ferrites.

Composition	$\nu_1(\text{cm}^{-1})$	$\nu_2(\text{cm}^{-1})$	$K_0$	$K_t$
$\text{CoFe}_2\text{O}_4$	558.42	528.0	$2.2 \times 10^5$	$3.2 \times 10^5$
$\text{CoEr}_{0.01}\text{Fe}_{1.99}\text{O}_4$	573.22	537.14	$2.3 \times 10^5$	$3.4 \times 10^5$
$\text{CoEr}_{0.02}\text{Fe}_{1.98}\text{O}_4$	609.39	524.52	$2.2 \times 10^5$	$3.6 \times 10^5$
$\text{CoEr}_{0.03}\text{Fe}_{1.97}\text{O}_4$	590.27	524.59	$2.2 \times 10^5$	$3.5 \times 10^5$
$\text{CoEr}_{0.04}\text{Fe}_{1.96}\text{O}_4$	573.22	524.49	$2.2 \times 10^5$	$3.3 \times 10^5$
$\text{CoEr}_{0.05}\text{Fe}_{1.95}\text{O}_4$	573.22	545.81	$2.4 \times 10^5$	$3.5 \times 10^5$

### 3.3. SEM studies

Ferrites surface morphology was analyzed by SEM which was used to match the crystallite size with existing XRD data. Figure 7 shows the distinctive SEM images of  $\text{CoEr}_x\text{Fe}_{2-x}\text{O}_4$  ( $x = 0.0, 0.01, 0.02, 0.03, 0.04, 0.05$ ) nano-crystallite. Micrographs of all compositions indicated that grains are well developed and crack free with clear grain boundaries, well packed. Monotony in the morphology was also shown by the surface. Additionally, the grains shapes were also analyzed which were cubic and almost spherical. Such type of morphology showed that grains possess a large surface area to volume ratio. This is the clear indication that the prepared nano-ferrites are effective microwave devices.

Fig. 7. SEM micrographs of  $\text{CoEr}_x\text{Fe}_{2-x}\text{O}_4$  ( $x = 0.0, 0.01, 0.02, 0.03, 0.04, 0.05$ ) spinel ferrites.

### 3.4. Dielectric properties

#### 3.4.1 Dielectric Constant and tangent loss

Dielectric properties are particularly important in order to reveal their applications for high frequency devices. Dielectric parameters like real and imaginary part of dielectric constant and tangent loss of  $\text{CoEr}_x\text{Fe}_{2-x}\text{O}_4$  ( $x = 0.0, 0.01, 0.02, 0.03, 0.04, 0.05$ ) were calculated. At frequency range of 1–3 GHz, the ferrites were studied at ambient temperature. It can be seen from Figure 8 (a) (b) that both dielectric steady and complex dielectric consistent diminished with the expansion of Er concentration. Both  $\text{Fe}^{2+}$  and  $\text{Fe}^{3+}$  particles assumed significant job in the polarization system of ferrites. Anyway  $\text{Fe}^{2+}$  particles assumed principle job in polarization and conduction process. Er particles developed on octahedral sites because of bigger ionic radii. Consequently, by adding the

Er, the number of Fe ions that explain the decrease in the dielectric constant is reduced. Due to the presence of a high concentration of secondary phase, the iron ions were reduced, thus the electron exchange mechanism between iron and iron ions was broken or deferred. As a result, the polarization and dielectric constant values were reduced by Er. There was also a significant correlation of hopping and the dielectric behavior of ferrites.

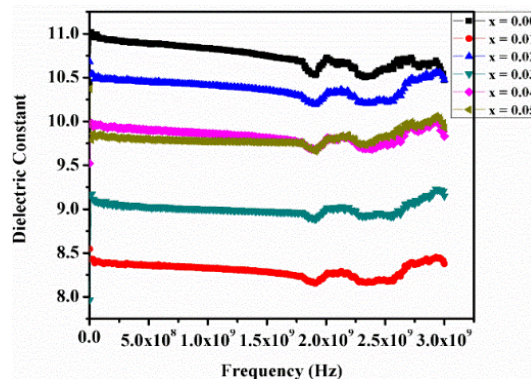


Fig. 8. Frequency dependent tangent loss.

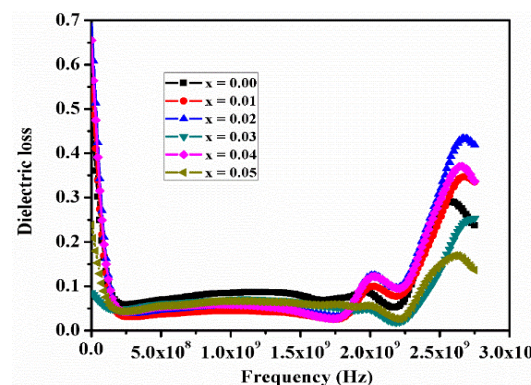


Fig. 9. Frequency dependent tangent loss.

### 3.4.2. Tan loss

The graph below shows the increasing concentration of Er and frequency, at higher frequencies the tangent loss is minimum. Tangent loss basically depends on the various factors such as sintering temperature, cation distribution at the tetra and octahedral sites and also stability of stoichiometry and structural homogeneity[24]. In Figure 10 it can be seen that as in case of high frequency upto 3 GHz, tangent loss has big variation. This may be possible due to exchange of electron between  $\text{Fe}^{2+}$  and  $\text{Fe}^{3+}$  at hopping frequency. Further, this exchange phenomenon is very difficult to monitor at high frequency. Due to this exchange on the adjacent octahedral sites define the maximum loss. This loss is determined when applied frequency is weaker than the hopping frequency. Spinel ferrites are basically anisotropic materials and have very high anisotropic field. Such high field has significant effect on the natural resonance that occurred in the high frequency region. It can be seen from figure that by increasing the substitution of ions, these peaks shift to the low frequency region. Hence, the resonance frequency decreases as the level of substitution increases.

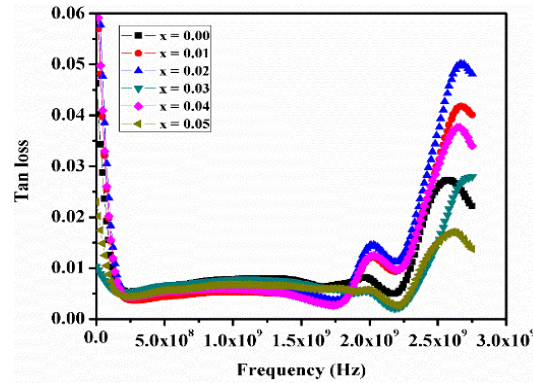


Fig. 10. Tan loss vs. Frequency for  $\text{CoEr}_x\text{Fe}_{2-x}\text{O}_4$  ( $x = 0.0, 0.01, 0.02, 0.03, 0.04, 0.05$ ) spinel ferrites.

Table 3. Effect of frequency on dielectric parameters of  $\text{CoEr}_x\text{Fe}_{2-x}\text{O}_4$  ( $x = 0.0, 0.01, 0.02, 0.03, 0.04, 0.05$ ) spinel ferrite.

Parameter	Frequency	X= 0.0	X= 0.01	X= 0.02	X= 0.03	X= 0.04	X= 0.05
Tan Loss	1.00 MHz	0.113	0.1157	0.128338	0.0997	0.0585	0.0544
	1.01 GHz	0.00823	0.00533	0.006567	0.00780	0.00588	0.00680
	3.00 GHz	0.00909	0.0229	0.01581	0.00869	0.0221	0.000586
Dielectric Constant	1.00 MHz	3.59	4.18	5.14	6.11	3.47	3.30
	1.01 GHz	4.18	5.05	5.38	5.72	3.80	3.59
	3.00 GHz	4.01	5.08	5.468923	5.85	3.79	3.67
Dielectric loss	1.00 MHz	0.404	0.656	0.63289	0.6.10	0.203	0.179
	1.01 GHz	0.0344	0.0270	0.035774	0.046	0.0223	0.0244
	3.00 GHz	0.0364	0.117	0.08375	0.0509	0.0837	0.00215
AC Conductivity	1.00 MHz	2.25E-05	3.65E-05	3.51E-05	3.39E-05	1.1E-05	9.96E-05
	1.01 GHz	0.00192	0.00151	0.002	0.00249	0.00125	0.00136
	3.00 GHz	0.00607	0.019	0.01396	0.0085	0.014	0.00358

### 3.4.3. AC Conductivity:

For high frequency device applications, dielectric parameters are very important for ferrites due to their high stability in polarization. These properties are basically depends on the approach or techniques to use for sample preparation, cation distribution at the octa and tetrahedral sides and also the annealing temperature.

The data of ac conductivity is determined by formula as follows

$$\sigma_{ac} = 2\pi f C_o D \quad (7)$$

Here “D” is the Loss co-efficient and “f” is the frequency and. It can be seen from Figure 11 that at low frequency no such significant effect was observed in ac conductivity, while that of at higher frequencies dispersion behavior is shown. In low frequency region, the high resistance is occurred in the plane and similar regions which have ultimately affect the grain boundaries. This behavior at low frequency defines the dielectric polarization which is very important for transmission process. Furthermore, the exchange of electron between  $\text{Fe}^{3+} / \text{Fe}^{2+}$  in the high frequency region at the adjacent octahedral regions play a vital role for AC conductivity. This phenomenon is governed by grain effect at high frequency. The magnitude of the electronic change relies on the concentration of the  $\text{Fe}^{3+} / \text{Fe}^{2+}$  ion pairs in the B site as shown in Figure 11.

These inspected dielectric parameters recommended the conceivable utilization of these nanomaterials in high recurrence gadgets.

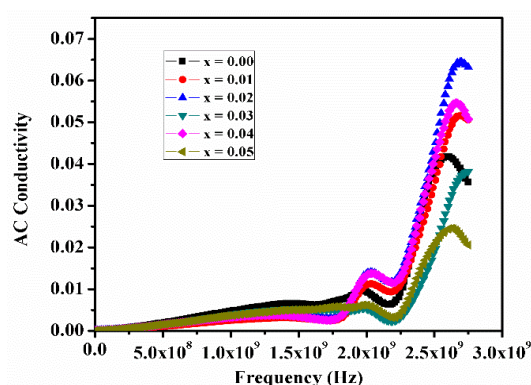


Fig. 11. Frequency dependent AC conductivity.

#### 3.4.4. Real and Imaginary Impedance

Impedance study is helpful to correlate dielectric parameters with microstructure. The complex impedance were determined for  $\text{CoEr}_x\text{Fe}_{2-x}\text{O}_4$  ( $x = 0.0, 0.01, 0.02, 0.03, 0.04, 0.05$ ). The variation in impedance were examined with effect of frequency are shown in Figures 12 and 13.

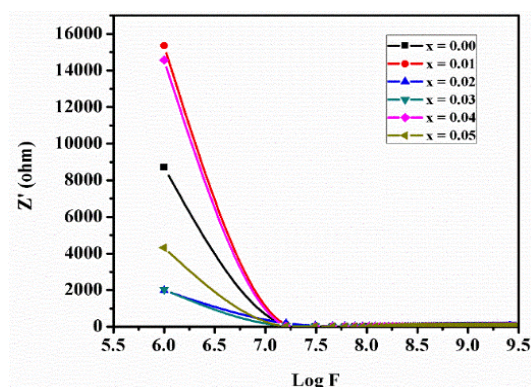


Fig. 12. Frequency dependent real part of impedance.

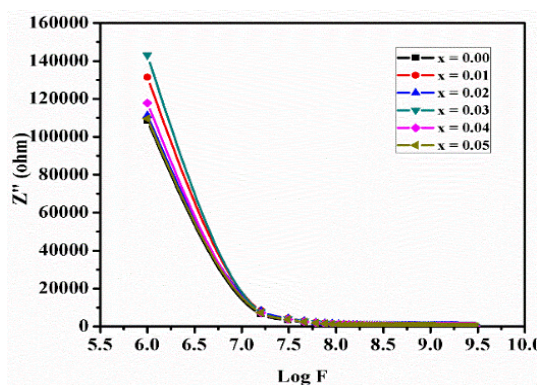


Fig. 13. Frequency dependent imaginary part of impedance.

The applied frequency has significant effect on the impedance. The decline in both impedance parameters was observed with increasing frequency. In case of frequency applied in

GHz, impedance exhibit constant trend due to release of space charge effect. These charges are due to the inhomogeneity of field and disparity in concentration and gathers in the bunch form at the grain boundaries. The determination of low impedance at high frequency has good correlation with AC conductivity.

### 3.4.5. Real and Imaginary Electric Modulus

The complex of electric modulus of composition formula  $\text{CoEr}_x\text{Fe}_{2-x}\text{O}_4$  ( $x = 0.0, 0.01, 0.02, 0.03, 0.04, 0.05$ ) are calculated. The formula used to find both parameters are:

$$M' = \varepsilon' / (\varepsilon'^2 + \varepsilon''^2) \quad (13)$$

$$M'' = \varepsilon'' / (\varepsilon'^2 + \varepsilon''^2) \quad (14)$$

Figs. 14 and 15 show the graph of real and imaginary modulus with the dependence of frequency ranging from 1MHz to 3GHz. The electric modulus is very crucial parameters that explain the effect of grain and grain boundaries. In addition, the purpose to find the electric modulus is to understand the interfacial polarization with influence of Erbium concentration in  $\text{CoEr}_x\text{Fe}_{2-x}\text{O}_4$  under the applied frequency range from 1MHz to 3GHz. This behavior can be confirmed by getting the relaxation peak due to relation of grain and grain boundaries at high frequency region. The relaxation peak observed can be seen in Figure 15. The calculated values of real and imaginary parts of electric modulus are summarized in Table 4.

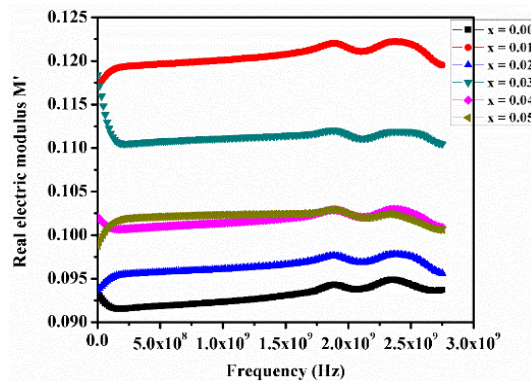


Fig. 14. Frequency dependent real part of electric modulus.

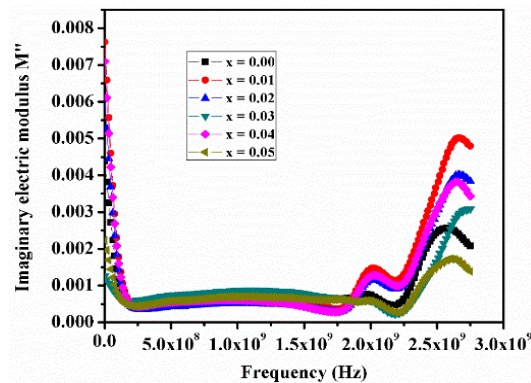


Fig. 15. Frequency dependent imaginary part electric modulus.

Table 4. Impedance and modulus values of  $\text{CoEr}_x\text{Fe}_{2-x}\text{O}_4$  ( $x = 0.0, 0.01, 0.02, 0.03, 0.04, 0.05$ ) spinel ferrite.

Parameters	Frequency	X=0.0	X=0.01	X=0.02	X=0.03	X=0.04	X=0.05
Z' (ohms)	1.00 MHZ	8.72E+03	1.54E+04	1.23E+04	2.02E+03	1.46E+04	4.31E+03
	1.01 GHZ	8.24E-01	7.37E-01	5.90E-01	9.80E-01	6.88E-01	7.94E-01
	3.00 GHZ	4.87E-01	1.14E+00	9.09E-01	5.18E-01	8.28E-01	4.39E-02
Z'' (ohms)	1.00 MHZ	108373.6	131495.3	105196.2	143021.5	117815.1	109647.1
	1.01 GHZ	104.5629	136.0066	108.8053	125.866	114.8295	115.8907
	3.00 GHZ	36.25099	45.29232	36.23386	41.48913	38.60384	38.23911
M'	1.00 MHZ	0.09515	0.115451	0.092361	0.125571	0.10344	0.096268
	1.01 GHZ	0.092325	0.120088	0.09607	0.111134	0.10139	0.102327
	3.00 GHZ	0.095483	0.119298	0.095438	0.10928	0.101681	0.10072
M''	1.00 MHZ	0.007652	0.013485	0.010788	0.001777	0.012792	0.003787
	1.01 GHZ	0.000727	0.000651	0.000521	0.000866	0.000607	0.000701
	3.00 GHZ	0.001283	0.002994	0.002395	0.001364	0.002181	0.000116

#### 4. Conclusions

In the current study, a series of sample with substitution of Erbium ion in  $\text{CoEr}_x\text{Fe}_{2-x}\text{O}_4$  ( $x = 0.0, 0.01, 0.02, 0.03, 0.04, 0.05$ ) spinel ferrites were synthesized through micro-emulsion route. X-ray diffraction analysis was employed in order to understand the structural properties of Erbium substituted cobalt spinel ferrites. XRD studies revealed that lattice parameters changed with the substitution of Er, which is because of Er ion has larger ionic radii as compare to ionic radii of Fe. XRD examination demonstrated that all samples have shown the stability in the prepared cobalt spinel structure. Furthermore, there are some secondary phase appeared this may be due to the larger ionic radii of Erbium. Crystallite size was found to be in nanometer regime. FTIR studies were performed to see the octahedral and tetrahedral bonding. The results confirmed the formation of  $\text{Er}^{3+}$  substituted cobalt ferrites. Dielectric parameters were measured in the applied frequency range of 1MHz to 3GHz using LCR meter. Moreover, with respect to concentration of Erbium there is dominant effect on dielectric, impedance, modulus and ac conductivity with respect to increase in Erbium content was observed. This shows the suitability of the material for high frequency devices.

#### Acknowledgements

We are grateful to ORIC of Balochistan University of Information Technology, Engineering and Management Sciences (BUIEMS), Quetta Pakistan.

#### References

- [1] J. Smith, H. Wijn, Ferrites, Eindhoven: Philips' Technical Library, (1959).
- [2] Z.A. Gilani, M.F. Warsi, M.A. Khan, I. Shakir, M. Shahid, M.N. Anjum, Physica E: Low-dimensional Systems and Nanostructures **73**, 169 (2015).
- [3] M.F. Al-Hilli, S. Li, K.S. Kassim, Journal of Magnetism and Magnetic Materials **324**, 873 (2012).

- [4] M. Yousefi, S. Manouchehri, A. Arab, M. Mozaffari, G.R. Amiri, J. Amighian, *Materials Research Bulletin* **45**, 1792(2010).
- [5] J. Kulikowski, *Journal of Magnetism and Magnetic Materials* **41**, 56 (1984).
- [6] S.H. Xiao, W.F. Jiang, L.Y. Li, X.J. Li, *Materials Chemistry and Physics* **106**, 82 (2007).
- [7] L. Kumar, M. Kar, *Ceramics International* **38**, 4771 (2012).
- [8] R.C. Kambale, K.M. Song, C.J. Won, K.D. Lee, N. Hur, *Journal of Crystal Growth* **340**, 171 (2012).
- [9] Z. Karimi, Y. Mohammadifar, H. Shokrollahi, S.K. Asl, G. Yousefi, L. Karimi, *Journal of Magnetism and Magnetic Materials* **361**, (1502014).
- [10] V.S. Puli, S. Adireddy, C.V. Ramana, *Journal of Alloys and Compounds* **644**, 470 (2015).
- [11] S. Wells, C.V. Ramana, *Ceramics International* **39**, 9549 (2013).
- [12] A.K. Nikumbh, R.A. Pawar, D.V. Nighot, G.S. Gugale, M.D. Sangale, M.B. Khanvilkar, A.V. Nagawade, *Journal of Magnetism and Magnetic Materials* **355**, 201 (2014).
- [13] I. Haïk Dunn, S.E. Jacobo, P.G. Bercoff, *Journal of Alloys and Compounds* **691**, 130 (2017).
- [14] I. Ali, M.U. Islam, M. Ishaque, H.M. Khan, M. Naeem Ashiq, M.U. Rana, *Journal of Magnetism and Magnetic Materials* **324**, 3773 (2012).
- [15] N. Sanpo, C. C. Berndt, C. Wen, J. Wang, *Acta Biomaterialia* **9**, 5830 (2013).
- [16] A. Goyal, S. Bansal, V. Kumar, J. Singh, S. Singhal, *Applied Surface Science* **324**, 877 (2015).
- [17] I. Nlebedim, N. Ranvah, P.I. Williams, Y. Melikhov, J.E. Snyder, A.J. Moses, D. Jiles, *Journal of Magnetism and Magnetic Materials* **322**, 1929(2010).
- [18] G.L. Hornyak, J. Dutta, H.F. Tibbals, A. Rao, *Introduction to nanoscience*, CRC press, 2008.
- [19] S. Gurav, S.E. Shirsath, R. Kadam, D. Mane, *Powder Technology* **235**, 485 (2013).
- [20] A. Zubair, Z. Ahmad, A. Mahmood, W.-C. Cheong, I. Ali, M.A. Khan, A.H. Chughtai, M.N. Ashiq, *Results in physics* **7**, 3203 (2017).
- [21] S. Prathapani, M. Vinitha, T.V. Jayaraman, D. Das, *Journal of Applied Physics* **115**, 17A502 (2014).
- [22] M. Srivastava, S. Layek, J. Singh, A.K. Das, H. Verma, A.K. Ojha, N.H. Kim, J.H. Lee, *Journal of Alloys and Compounds* **591**, 174 (2014).
- [23] Z.A. Gilani, M.F. Warsi, M.A. Khan, I. Shakir, M. Shahid, M. N. Anjum, *Physica E: Low-dimensional Systems and Nanostructures* **73**, 169 (2015).
- [24] R. Nongjai, S. Khan, K. Asokan, H. Ahmed, I. Khan, *Journal of applied physics* **112**, 084321 (2012).